ANL-4602

SECRET

Argonne National Laboratory

QUARTERLY REPORT FOR DECEMBER 1950, JANUARY AND FEBRUARY 1951

PHYSICS DIVISION

SECRET

DISCLAIMER

ARGONNE NATIONAL LABORATORY
P. O. Box 5207
Chicago 80, Illinois

* * * * *

REPORT FOR DECEMBER, 1950, JANUARY AND FEBRUARY, 1951

PHYSICS DIVISION

Louis A. Turner, Division Director

* * * * *

Preceding quarterlies: ANL-4437 January, February, and March 1950
ANL-4476 April, May, and June 1950
ANL-4515 July, August, and September 1950
ANL-4552 October, and November 1950

March 5, 1951

Operated by the University of Chicago

under

Contract W-31-109-eng-38

Distribution	Copy No.
Argonne National Laboratory	1- 38
Armed Forces Special Weapons Project	39
Atomic Energy Commission	40- 45
Brookhaven National Laboratory	46- 49
Bureau of Ships	50
Carbide & Carbon Chemicals Div.(K-25)	51- 52
Chief of Naval Research	53
Columbia University (Dunning)	54
E. I. du Pont du Nemours & Co.	55- 58
General Electric Company, Richland	59- 64
Hanford Operations Office	65
Idaho Operations Office	66- 67
Iowa State College	68
Knolls Atomic Power Laboratory	69- 72
Los Alamos	73- 75
Mound Laboratory	76- 77
National Advisory Comm. for Aeronautics	78
Naval Radiological Defense Laboratory	79
Naval Research Laboratory	80
NEPA Project	81
New York Operations Office	82- 83
North American Aviation, Inc.	84
Oak Ridge National Laboratory, X-10 Site	85- 92
Patent Branch, Washington	93
Savannah River Operations Office	94
Technical Information Service, Oak Ridge	95-109
UCLA Medical Research Laboratory (Warren)	110
USAF - Headquarters	111
University of California Radiation Lab.	112-114
Westinghouse Electric Company	115-118
Total	118

TABLE OF CONTENTS

TABLE OF CONTENTS CONTIN.:

979-B

Group #1 - C. O. Muehlhause

1. Neutron Transmission and Scattering Cross Sections (C. T. Hibdon)

Using the annular scattering counter with various scattering detectors, transmission curves of a number of elements were measured. Table I lists new data. Cross sections are given in barns at the energies indicated. The number in parenthesis indicates the percentage of the transmission curve exhibiting the asymptotic cross section. A low value of this percentage indicates considerable overlapping of resonance regions of the absorber and detector. When no such number is given the transmission curve is a straight line on a semi-log plot (c.f. previous quarterly reports). In certain cases the thermal and epi-cadmium cross sections were also measured. The first of these is obtained by comparison with V^{51} ($\sigma_{ths} = \sigma_{inc} \cong 5.00$ b) which has no crystal interference effects, and the second is obtained, as previously outlined, by comparison with C ($\sigma_{epi-cd} \cong 4.60$). The measurements on hydrogen were obtained with Lucite (L) and Polystyrene (P). These have yet to be corrected for possible impurities, C-H-O ratio and potential scattering of the detector. In what follows, certain details of Table I will be amplified and discussed.

A. Cobalt shows remarkable resonance overlapping with vanadium, 78% (1.00-0.22). This is almost as much as vanadium shows by self-indication ($\sim$ 82%). One can only conclude that Co and V each have resonances within about 100 ev. Furthermore since Na, V, Mn and Co show large mutual overlapping, all these resonances must be close to 3000 ev. This is in disagreement with the data of Columbia's neutron velocity selector which locates the second Co resonance(s) at 7800 ev. From past experience we would expect this second Co resonance to involve scattering primarily. However, the following experiment was performed and indicates that the main process at the 2700 ev Co resonance is absorption. The epi-cadmium

TABLE I

Element	σ_{ths}	σ_{epi-cd}	10.0 ev (Sm^{152})	19.5 ev (W^{186})	120 ev (Co^{59})	2400 ev 345 ev (Mn^{55})	2700 ev (V^{51})	3000 ev (Na^{23})	3800 ev (Cr^{53})
$_{1}H$			20.09(L) 20.49(P)						
$_{22}Ti$								5.02	
$_{26}Fe$								7.00	
$_{27}Co$	8.34		10.29	8.52(65)			4.09(22)	4.55(46)	
$_{32}Ge$			5.13	4.08	4.93	4.01	2.54(91)		4.47
$_{33}As$							7.35(86)	6.77(77)	
$_{40}Zr$				6.23	6.30	5.83(87)	6.03(85)	6.23(89)	
$_{47}Ag$	5.72	13.83							
$_{72}Hf$			17.0 (83)		13.1 (71)	14.4 (71)	14.8 (73)	14.8 (67)	
$_{74}W$							8.45(68)	8.31(69)	
$_{79}Au$	7.56								
$_{80}Hg$	26.56	19.06	13.93	13.3			10.4 (67)	10.7 (68)	

scattering cross section of Co was measured with and without a thick V filter in the neutron beam. Very little drop in σ_{epi-cd} resulted when V filtering was employed:

$$\sigma_{epi-cd}\ (Co) - \text{no V} = 42.6$$

$$\sigma_{epi-cd}\ (Co) - \text{with V} = 42.0$$

i.e. $\Sigma_{s\ 2700}\ (Co) \simeq 8.4\ (42.6 - 42.0)/.50 \simeq 10$ b

This is very small compared with the integral values of Na, V, and Mn at this same energy, yet the Co 2700 ev resonance is able to remove practically all of the rather broad V resonance scattering with a Co filter of reasonable thickness. For comparison:

$$\Sigma_{s\ 3000}\ (Na) = 51 \text{ b}\quad \Sigma_{s\ 2700}\ (V) = 192 \text{ b}\quad \Sigma_{s\ 2400}\ (Mn) = 90 \text{ b}$$

Additional work will be carried out on the resonance absorption of Co to test this view. It is of interest to note, however, that the thermal absorption cross section of Co is too large to be properly accounted for by the 120 ev resonance alone.

In addition to the above considerations, it is interesting to calculate the scattering cross section of Co at 10.0 ev and 19.5 ev from the data in Table I. To do this it is permissible to assume a 1/v dependence of capture:

$$\Sigma_s\ (Co\text{-}10 \text{ ev}) \simeq 10.29 - \frac{34.8}{\sqrt{40.10}} \simeq 8.55 \text{ b}$$

$$\Sigma_s\ (Co\text{-}19.5 \text{ ev}) \simeq 8.52 - \frac{34.8}{\sqrt{40.19.5}} \simeq 7.29 \text{ b}$$

Thus, the scattering cross section appears to be rising in the low energy region. This is difficult to understand without postulating a third resonance level below binding. It is important to remeasure the thermal scattering cross section.

B. Gold - There has been some question in the past about the thermal

scattering cross section of gold. The difficulty is one of crystal effects. The value given in Table I is uncertain for this reason. However, two pieces of outside evidence support our measurement: (1) the data of Titman and Shears (Columbia neutron velocity selector) would indicate an incoherent cross section of only 0.3 b, (2) the work of Shull (Oak Ridge) gives the coherent scattering cross section, a value of 7.5 b. Therefore, $\sigma_{ths} = 7.5 + .3 \simeq 7.8 \pm .5$ b.

C. The cross sections for thermal absorption and scattering of mercury are governed by a resonance at -2.0 ev in Hg^{199}. Inspection of Table I will reveal that even $\sigma_{epi-cd} < \sigma_{ths}$. Ringo and Robillard (cf. page 14 of this report) report $\sigma_{coh} = 21.5 \pm 2$ b. Using only thermal values (i.e., the above and $\sigma_{tha} = 370$ b) it is possible to calculate resonance parameters for the -2.0 ev level. To do this one proceeds on the assumption that the radii are spin independent and identical for all the mercury isotopes. One then obtains two parameter sets corresponding to $J = 0$ or $J = 1$ ($I = \frac{1}{2}$ for Hg^{199}). These are given in Table II. The best value of $4\pi R^2$ appears to be for the case $J = 1$, since at 19.5 ev the measured cross section is 13.3 b. If one assumes this latter value to be $4\pi R^2$ and calculates σ_{coh} one obtains a different set of resonance parameters. These are given in Table III. Again $J = 1$ is preferred, but $J = 0$ cannot be ruled out with absolute certainty.

An interesting consequence in the choice of J for nuclei with initial spin $\frac{1}{2}$ has to do with the resulting capture γ-ray spectrum. The compound nucleus in this case is $_{80}Hg^{200}$, an even-even nucleus with ground state angular momentum equal to zero. Therefore, a γ-ray transition of energy equal to binding in Hg^{200} is forbidden for $J = 0$ and allowed for $J = 1$. Furthermore, the first transition in the cascade is usually of sufficient energy that no other γ-ray will be likely to be confused with the total

Table II

Hg^{199} ($\sigma_{coh} = 21.5$ b)

	J = 0	J = 1
Γ_n	0.03888 ev	0.02349 ev
Γ_γ	0.3081 ev	0.1700 ev
Γ	0.3470 ev	0.1935 ev
Γ_n/Γ	0.112	0.121
R	1.1753 $b^{\frac{1}{2}}$	1.0674 $b^{\frac{1}{2}}$
$4\pi R^2$	17.36 b	14.32 b

Table III

Hg^{199} ($4\pi R^2 = 13.3$ b)

	J = 0	J = 1
Γ_n	0.05332 ev	0.02678 ev
Γ_γ	0.2247 ev	0.1491 ev
Γ	0.2780 ev	0.1759 ev
Γ_n/Γ	0.192	0.152
σ_{coh}	17.1	20.0

transtion. B. Hamermesh reports no structure in the high energy end of the capture γ-ray spectrum of Hg^{199} + n. This would indicate J = 0 for the capture state, i.e., the - 2.0 level, whereas the present work favors J = 1.

2. Internal Conversion of Capture γ-Rays (C. T. Hibdon)

The electron spectrograph described in the previous quarterly report has yielded well-resolved conversion lines from capture γ-rays of Gd and Sm. Results are given in Table IV.

Table IV

Element	Isotope	E_e	K	L_2	L_3	M	E_γ
Gd	155 and 157	30.1	80.5				81.0
		39.7	90.1				90.2
		73.3		81.2			
		74.1			81.3		
		79.7				80.9	
		83.4			90.6		
		135	185				185
Sm	152	294	341				341

3. Resonance Region Time-of-Flight Measurements (S. P. Harris)

Additional runs of a preliminary nature have been made on certain materials of interest. Since a new higher speed rotor is soon to be put into operation (allowing 2 μs channels instead of 3 μs) an intensive effort to locate resonances in the neighborhood of 3000 ev more accurately is being withheld for that later time. Table V lists certain results obtained this quarter.

Table V

Sample	Thickness gm/cm^2	Resonance Energy ev	Comment
$_{23}V^{51}$	3.28	3300 $^{+1500}_{-750}$	av of 3 runs
$_{27}Co^{59}$	8.04	3600 $^{+1800}_{-900}$	av of 2 runs
		120	
$_{33}As^{75}$	6.25	43 ± 3.5	weak unresolved resonances at higher energies
$_{75}Re$	2.97	18.0 10.8 7.1 5.7	13 ev res. of columbia not observed. May be due to Pt.
$_{75}Re^{187}$	1.45	10.8	Only res. observed below 25 ev

From the velocity selector data to date no distinction in energy between the resonances in Na, V, and Co near 3000 ev can be made. The amount of overlapping of Mn with these materials, however, places the second Mn resonance at a lower energy than that of the Na - V - Co group.

Rhenium has two isotopes (185, 187). The above runs were limited to 25 ev. Apparently the 10.8 ev level belongs to Re^{187} and the 18.0, 7.1, and 5.7 ev levels belong to Re^{185}.

Earlier work on arsenic by Harris, Hibdon, Muehlhause and Thomas indicated a fairly low energy resonance having about 70% scattering. This would not be unreasonable for the 43 ev level.

4. Pile Oscillator Circuit (C. O. Muehlhause)

Since the change in CP-3 has been effected the pile oscillator has become a superior cross section measuring instrument (c.f. quarterly report for October-November, 1950). It was, therefore, decided to

improve the detection circuit. To date the effect of a sample is measured in terms of a resistance, R_1, which oscillates in and out of a bridge circuit (in phase with an absorber or 180° out of phase with a neutron source). This is illustrated in Fig. 1

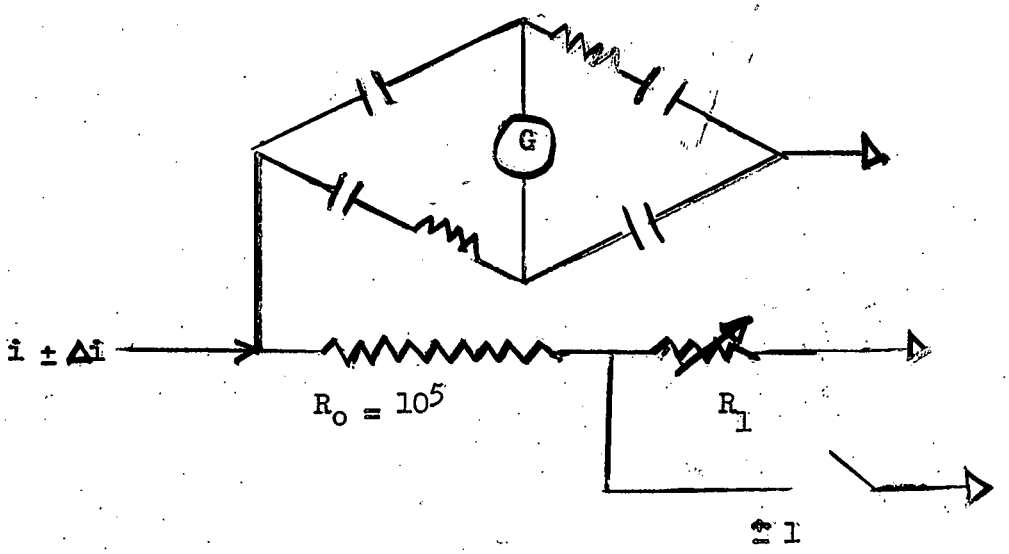

Fig. 1

Adjustment of R_1 for null yields $\Delta i/i$ which is proportional to cm^2 absorption of the sample. However, the above amounts to an attempt to balance the pile wave form with a square wave:

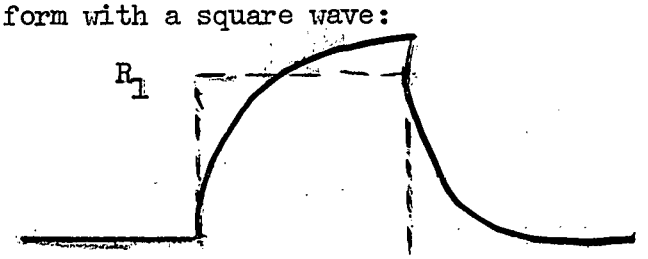

This results in the leaving over of a second harmonic which causes the galvanometer spot to oscillate about null with twice the frequency of the sample.

An obvious extension of the above is to add still another resistance, R_2, which will oscillate in and out of the bridge circuit 90° out of phase with R_1. This makes it possible to achieve a step function match to the

pile wave form:

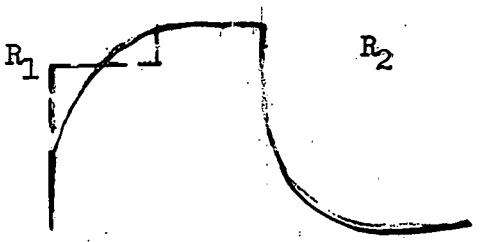

The ratio, R_2/R_1 should be $\sim \delta/T$, where δ is the effective rise time of the pile wave and T is the half cycle time of the oscillation. When R_1 and R_2 are both adjusted the fourth harmonic should be evident, and the null galvanometer spot should have less of an amplitude about zero. The basic diagram of the new circuit is illustrated in Fig. 2.

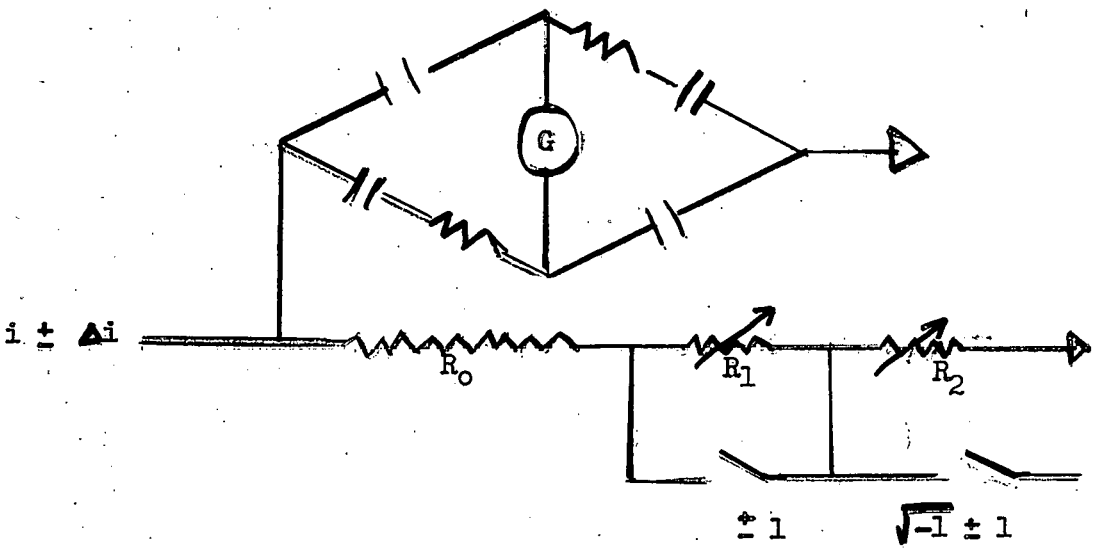

$$cm^2 \text{ (sample)} \propto \frac{\frac{R_o}{2}\ (R_1 + R_2)}{R_o + \frac{1}{2}\ (R_1 + R_2)}$$

II. Coherent Neutron Scattering by Mercury (G. R. Ringo and T. R. Robillard)

The coherent neutron scattering cross section of mercury has never been measured previously because its very high absorption cross section makes measurements by the usual crystal diffraction techniques very difficult. As a by-product of work on the coherent amplitude of hydrogen using liquid hydrocarbon mirrors, the coherent amplitude of mercury was measured using the same apparatus. It was measured by finding the critical wavelength for reflection of a beam of thermal neutrons incident on a surface of liquid mercury at a given angle. This was found at two angles by use of the Brill and Lichtenberger time-of-flight velocity selector and at a third larger angle by comparison of intensities with the first two angles, knowing the spectrum of the neutron source. The source was the thermal column of CP-3. The critical wavelength and the angle determine the index of refraction, and this determines the coherent scattering amplitude.[1] The results are summarized in the table.

Angle in Minutes	Wavelength in Angstroms	Coherent Cross Section in Barns
8.29±.05	1.84±.1	22.1±2
17.25	2.63±.2	24.8±3
20.22	4.70±.5	18.4±4
	thermal average	21.5±2

The variation with wavelength is not thought to be significant in view of the uncertainties (which come largely from the relatively poor statistics). As can be inferred from the large coherent cross section, mercury makes a very good mirror for neutrons. It has a surface that is easily prepared and is stable for at least several days with only ordinary care.

1. E. Fermi and L. Marshall, Phys. Rev. 71, 666 (1947)

III. Incoherent Scattering of Slow Neutrons from Spin Dependent Interactions (M. T. Burgy)

Spin dependence of the interaction between a neutron and an atomic nucleus introduces an incoherence in the scattering with a cross section proportional to the absolute square of the difference of the scattering amplitudes, a_+ and a_-, corresponding to the two states of total angular momentum $I + \frac{1}{2}$ and $I - \frac{1}{2}$, where I is the nuclear spin. A part of this incoherent scattering involves spin flip of the neutron and nucleus, and where the incident neutron beam is polarized, the spin flip changes the polarization. All other forms of incoherent nuclear scattering and the coherent scattering do not change the polarization of the neutrons. Thus a comparison of the polarization of a scattered beam with that of the incident beam provides a means of measuring the incoherent scattering cross section due to spin dependence of the interaction.

This cross section, together with the coherent or free atom scattering cross section, determines a set of possible values for the two amplitudes a_+ and a_-. The same information is obtainable from the values of the coherent and free atom cross sections together, but where the spin dependence is small, its calculation from these two numbers is subject to large errors since a small difference is involved.

The method considered involves scattering a polarized beam of slow neutrons by a sample of a substance to be studied and counting those which pass through an analyzing block of strongly magnetized cold rolled steel. A measure of the polarization of the scattered beam is obtained from the change in transmission of the analyzer when the scattered beam is depolarized by a thin sheet of unmagnetized steel. The polarization of neutrons scattered incoherently due to spin dependence of the interaction is -1/3 of the initial polarization, P_0, while in the rest of the scattering the initial polarization

is unchanged. If σ_s is the total scattering cross section for the solid angle of observation and σ_f the incoherent scattering cross section from the spin dependence, the polarization P_s observed is given by

$$P_s = \left((\sigma_s - \sigma_f) P_0 - 1/3 \sigma_f P_0 \right) / \sigma_s = (1 - 4/3 \frac{\sigma_f}{\sigma_s} P_0 .$$

A measurement of the polarization of the incident beam is made in the same way as for the scattered beam, and from the two the ratio σ_f/σ_s is obtained. The value of σ_s is obtained from the observed counting rates of the direct and scattered beams, the solid angle of observation and the total cross section.

At present, some preliminary observations are being made to check the feasibility of such measurements and serve as a basis for design of equipment. A magnetized cobalt mirror was tried as the polarizer in one setup, but the intensity of scattered neutrons obtained was too low. In another setup, the polarization of the incident beam was achieved by transmission through strongly magnetized cold rolled steel, and a counting rate of about 5000 counts per minute of scattered neutrons above background was obtained. With paraffin as the scattering substance, a change in polarization in scattering which agrees with that expected from the values of the coherent and free atom cross sections has been observed in a first rough measurement.

IV. Activities of Hf Isotopes (S. B. Burson)

From measurements made using the enriched isotopes of Hf, obtained from the Oak Ridge National Laboratory, definite isotopic assignments of each of the four activities were made and accurate energy values for the gamma-rays determined; the results are summarized in the table:

	Activity	Process	Gamma-ray Energies in Kev
$_{72}Hf^{181}$	(45 d)	420 kev β^-	611, 481, 344, 136, 133
$_{72}Hf^{180*}$	(45.5 h)	Isomeric	442, 330, 214, 93.2, 56.8
$_{72}Hf^{179*}$	(19 s)	Isomeric	161
$_{72}Hf^{175}$	(70 d)	K-capture	342, 228, 113, 89.1 (The line previously reported in ANL-4552 at 53.0 was found to be attributable to Auger electrons due to the high intensity of K X-rays resulting from K electrom capture.)

It should be noted that the presence of an isomeric state in $_{72}Hf^{180}$ is a violation of "Mattauch's rule" which states that isomeric states are not generally found in nuclei of both even atomic number and even mass number.

V. Internal Conversion Spectra of Radioisotopes (W. C. Rutledge)

A study of the internal conversion electron spectra of several radioisotopes was conducted in a magnetic spectrograph. Enriched isotopes of selenium and samarium were used. An especially purified sample of thorium oxide was obtained from the Chemistry Division. The results given below represent only what has been completed so far.

Radio-isotopes	Associated Half Life	Mode of Decay	Electron Energy	Inter pretation	Energy Sum (Kev)	Gamma Energy (Kev)
Se^{79}	16 m	Isomeric Transition	83.2	K	95.9	
			94.2	L	95.8	95.9
Se^{81}	58 m	Isomeric Transition	90.5	K	103.2	
			101.4	L	103.0	103.1
Sm^{153}	46 h	β	21.2	K	69.9	
			33.5	Auger L_I	α_2	
			39.8	Auger M	α_2	
			54.7	K	103.4	
			61.7	L_I	69.8	
			62.9	L_{III}	69.9	
			68.1	M	69.9	
			69.3	N	69.7	69.9
			95.3	L_I	103.4	
			101.5	M	103.3	
			102.9	N	103.3	103.4
Sm^{155}	23 m	β	56.0[5]	K	104.7	
			96.6	L_I	104.7	
			104.4	M	104.8	104.7
		Isomeric Transition	197.2	K	244.2	
			236.4	L_I	244.2	244.2
Th^{233}	23 m	β	None, except those in the electron spectrum of Pa^{233}.			
.3 → .6% Eu contaminant in samarium isotopes	9 h	K-capture	75.1	K	122.0	
			114.2	L_I	122.0	
			114.7	L_{III}	122.0	
			120.1	M	121.8	
			121.4	N	121.8	121.9

VI. Low Voltage Accelerator Activities (L. S. Goodman)

The following total cross sections have been measured for D-T (14 Mev) neutrons.

The detection and monitoring were done with anthracene crystal scintillation counters.

The cross sections have been corrected for room scattering (3%) and "in-scattering" (.2%).

H	.68 ± .05	b
C	1.14 ± .04	b
O	1.49 ± .11	b
Mg	1.83 ± .18	b
Al	1.67 ± .1	b
Ti	2.25 ± .2	b
V	2.38 ± .12	b
Cr	2.33 ± .2	b
Fe	2.33 ± .2	b
Ni	2.41 ± .1	b
Cu	2.46 ± .1	b
Zn	2.88 ± .2	b
Zr	3.5 ± .2	b
Mo	3.6 ± .3	b
Sn	4.02 ± .38	b
Sb	4.6 ± .25	b
W	4.62 ± .3	b
Pb	5.0 ± .35	b
Bi	5.13 ± .5	b

VII. Van de Graaf Generator (A. S. Langsdorf, Jr.)

A number of changes and improvements have been made in the accelerating tube and belt charging system of the Van de Graaf generator.

The pressure sensitive leaks which caused serious trouble last fall have been eliminated by the replacement of several punctured porcelain tube sections. Following upon this work, much effort was expended in properly aligning the accelerating tube and ion source so that the beam would be more nearly on the axis of the tube. After success in this undertaking, 14 diaphragms were inserted at about equal intervals into the electrodes of the accelerating tube. The two diaphragms nearest the ion source have a 2" aperture and the remaining 12 have a 3" aperture. A well focused beam can now be obtained through the system. These diaphragms have improved the behavior of the accelerating tube, apparently by decreasing current loading in it. The best evidence for this improvement is that the meters which read current returning down the needle gaps of the column all read about alike, whereas formerly they read very different amounts of return current. It is logical to infer that the current which disappeared had gone into ion currents inside the accelerating tube. Direct proof of such phenomena, however, is very difficult to obtain.

Following upon this work, improvement of the belt charging system was undertaken. During the past two years, the machine had been operated with one needle bar at the ground end spraying charge on and one needle bar at the high voltage end taking charge off. Attempts to use self-induction at the high voltage end in order to send negative charge down the return run of the belt had not been successful in the past. The reasons for this failure were extensively studied and steps taken to rectify the difficulty. The major reason for the difficulty was located. It is that there is not sufficient space between the belt and metal structures in and near the

high voltage end of the machine to build up adequate potential between the belt and the wiper needle bar. It was possible to obtain adequate wiping of positive charge in open air and in pressures up to about 50 pounds. However, at higher pressures it was not possible to remove sufficient positive charge from the belt to maintain the pulley at a sufficient positive voltage to induce negative spraying onto the belt for the return run. This difficulty has now been handled with fair success by a scheme of charging the pulley with a voltage obtained from the beam focusing voltage system. Recently, we have been able to obtain adequate negative return current on the belt at 100 pounds pressure with all indications that it will work at even higher pressures.

Another necessary adaptation has been accomplished to obtain sufficient focusing potential in the high voltage shell to focus the beam with the machine above 3 million volts. There was need for more initial acceleration of the ions from the arc than could conveniently be obtained from a rectifier power supply. The basic reason for this difficulty is the great distance between the ion source and the beginning of the accelerating column in our generator as compared to other electrostatic generators. It appears now that a simple initial acceleration of ions would need from 80 to 100 kv, but it is not convenient to make a rectifier supply for more than about 50 kv and our present supply is limited to 40 kv. About a year ago an extra accelerating gap (and lens) was installed between the end of the accelerating tube and the initial accelerating electrode beyond the probe. This gap improves operation by decreasing the required focus voltage from the rectifier power supply. However, the voltage for this additional acceleration was obtained from the potential on the pulley and the ability of this part of the electrostatic system to handle the necessary current has turned out to be inadequate.

A way out of this difficulty was found by Mr. Holland: There is now an additional adjustable corona needle gap between the needle bar which sprays negative charge on to the belt and high voltage shell. The needle bar itself is connected to the accelerating electrode system and supplies the desired additional accelerating voltage. This system is capable of providing all the needed current as well as maintaining the desired voltage. A schematic diagram of the present system of needle bars and adjustable gaps is given in Figure 3.

One additional and fairly successful feature of the belt charging system is shown on this diagram. This is the needle bar and adjustable gap denoted as the degeneration system. This needle bar faces the belt after it has left the pulley on the return run carrying negative charge. It can be so set that when an adequate negative charge is returning down the pulley any excess negative charge above that desired flows from the belt to the needle bar and back through the adjustable gap to the pulley in such a manner as to decrease the positive potential on the pulley and thereby to decrease the amount of negative charge sprayed onto the belt. This system is inherently degenerative in its action and permits one to set the negative return current to a desired value without the adjustment being extremely critical as it would otherwise be.

In the past few weeks, the machine has been operated up to 3.2 million volts at 75 pounds pressure and more recently to 3.5 million volts at 100 pounds pressure. During some of these tests there was a limitation on voltage as a result of some loose hoops on the center section of the machine. The defective assembly of hoops has been corrected. The The charging system and column of the machine should certainly be able to permit operation up to or above 4 million volts.

The proton beam is exceedingly stable and the machine more easy to

hold in control than at any time in the past, at least up to 3.4 million volts. The former fluttering of the voltage, even under control, has been eliminated almost entirely and the voltage of the machine does not wander from its setting as it formerly did, even when it is not being controlled. A beam current of 10 microamperes of protons was easily obtained and there is a large reserve of ability of the ion source to supply more. The present limit of the machine near 3.5 million volts seems to be set by some form of breakdown, most probably in the differential pumping tube. An attempt to improve this tube will be made by increasing the number of diaphragms in this tube to fourteen from the present number (six).

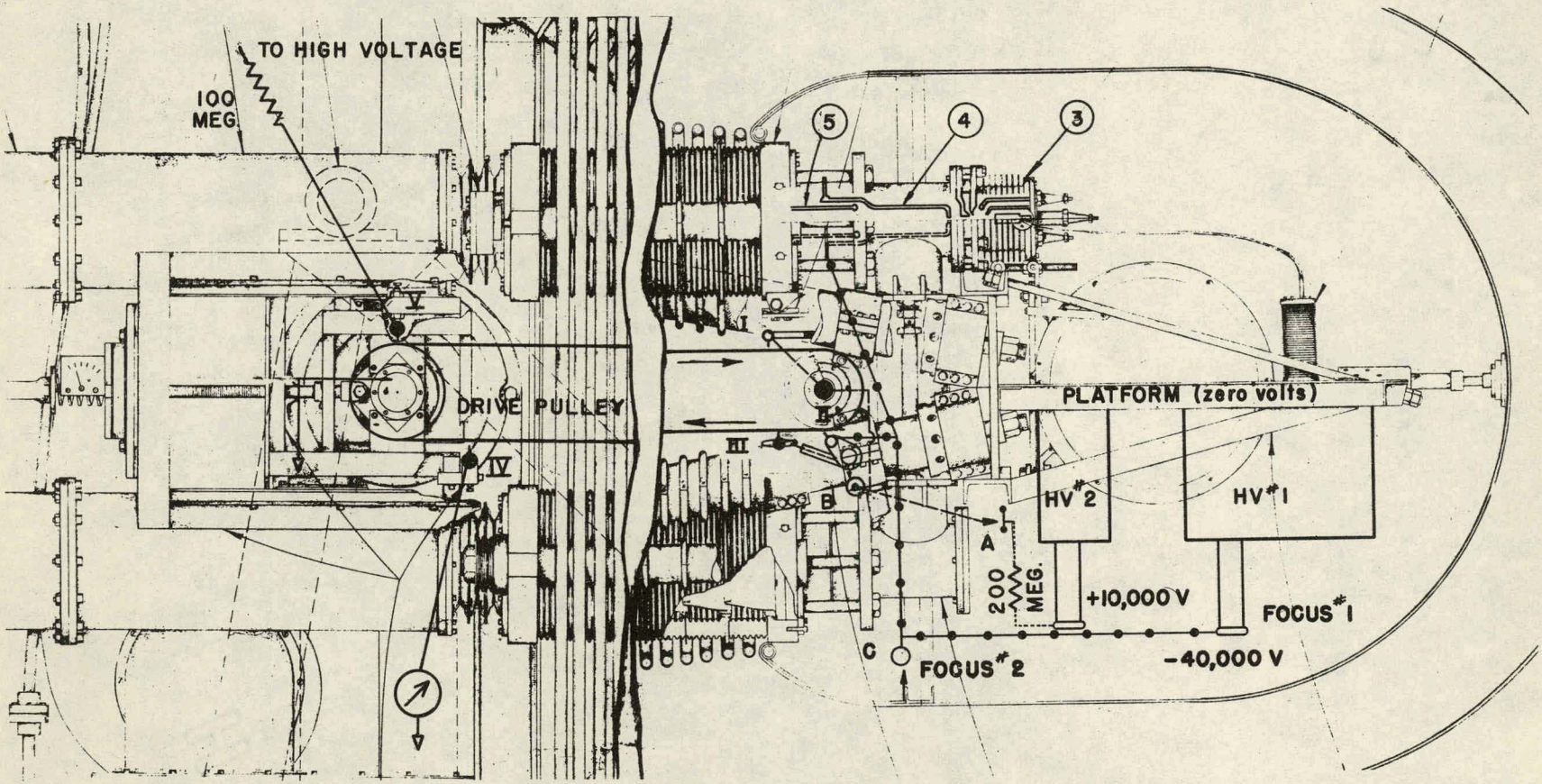
TO HIGH VOLTAGE
100 MEG.
V
DRIVE PULLEY
IV
III
I
II
5
4
3
PLATFORM (zero volts)
HV #2
HV #1
A
B
C
200 MEG.
+10,000 V
FOCUS #1
FOCUS #2
-40,000 V

Fig. 3

Figure 3

The needle bars which spray charge onto the belt are indicated by Roman numerals I through V. The first one, I, is intended to remove positive charge from the belt. It is electrically connected to the pulley. The intention is that this charging current will make the pulley positive enough to induce negative spray onto the belt by needle bar II. The failure of this self-induction to operate properly is overcome by the use of HV #2 supply and adjustable needle gap "A".

Needle bar III is called the degeneration bar because it limits the amount of negative charge returning down the belt. It does this by picking up negative charge and returning it to the pulley via adjustable needle gap "B", thus limiting how positive the pulley can become and limiting negative spray to the belt by needle bar II.

Needle bar IV removes most of the negative return current from the belt at the ground end of the machine. Needle bar V sprays positive charge onto the belt for the up-run to the high voltage end. The 100 megohm resistor in the line to needle bar V helps materially to hold the positive spray at a constant value.

There are three adjustable corona needle gaps in the high voltage shell of the machine, labelled "A", "B", and "C". Gap "A" controls the induction potential of the pulley by regulating the charging current to the pulley from the positive potential supplied by the two high voltage supplies (HV #1 and HV #2) in series. The 200 megohm resistor in the line from gap "A" to HV #2 helps smooth the nonlinearity of voltage versus current across gap "A", and is intended to help stabilize the induced negative spray from needle bar II. Gap "B", as already mentioned, regulates the degeneration and limits the negative return current on the belt. Gap "C" is adjusted to focus the beam. It supplies the potential called "focus #2"

voltage which appears at the gap between electrodes marked no. 4 and no. 5 in the accelerating tube.

Gap "C" and the "focus #2" voltage it supplies reduces materially the voltage required from the high voltage supply, HV #1, in order to focus the beam properly at the target. Without "focus #2" voltage, more than the 40,000 volts actually available from HV #1 would be needed to focus the beam at 3.5 Mev machine output voltage. The HV #1 potential is called "focus #1" voltage and is also externally adjustable. This voltage appears in the accelerating tube between the electrode marked no. 4 and the arc source, no. 3. (Actually the probe electrode lies between the arc body and the electrode no. 4. The probe is usually about 1500 volts negative with respect to the arc.)

VIII. Group #2 - S. Wexler

1. Fraction of Positive Charged 18 min Br^{80} Atoms from Isomeric Transition (S. Wexler)

Two γ-rays are emitted when 4.5 hr Br^{80m} decays to its 18 min daughter. The 49 kev gamma is completely converted while the 37 kev ray is about half converted.[1,2] Since the internal conversion process ejects an extra nuclear electron, the product atom should acquire a positive charge. Subsequent Auger processes should increase the magnitude of the charge. Thus, in the case at hand, the isomeric transition of Br^{80m}, every 18 min bromine should be positively charged. But only 50-70 per cent of the transitions were observed to yield Br^+ when C_2H_5 Br^{80m} at a few microns pressure was allowed to decay between charged copper-amalgam electrodes.[3] Neither a five-fold increase in ethyl bromide pressure nor a seven-fold decrease of mercury pressure altered the results appreciably. Change to phenyl bromide as the Br^{80m} bearing compound had no effect on the fraction of positive bromines. However, the yield of Br^+ doubled on increasing the collecting voltage from 90 to 1000 volts.[4] Therefore, interest in the effect of a much higher electric field arose.

Three experiments were performed in which the positive decay atoms were collected on a 1.6 mm diameter rod by a potential of 20 kv. The rod was surrounded by a coaxial cylinder 20 mm in diameter. Experimental procedures and techniques have been described[3] but two significant changes were made. The electrical leads to the rod and wall respectively were brought in through opposite ends of the decay chamber. In addition, hydrogen-reduced copper rather than Cu-amalgam electrode surfaces were employed. The procedures for H_2 reduction is described in earlier work.[5]

---

1. A. P. Grinberg and T. I. Roussinow, Phys. Rev. 58, 181 (1940).
2. P. Rothwell and D. West, Proc. Phys. Soc. 63, 539 (1950).
3. S. Wexler and T. H. Davies, J. Chem. Phys. 18, 376 (1950).
4. S. Wexler and T. H. Davies, ANL-4397.
5. S. Wexler and T. H. Davies, ANL-4515.

The results are collected together in Table VI. Columns 2 and 3 give the 18 min Br^{80} activities found on the rod and wall respectively, corrected for chemical yield and a small 4.5 hr activity, while column 4 gives the ratio of wall to rod counting rates. Conversion of the experimental wall to rod ratios to fraction of positive bromines is made through the following equations:

$$R_o = \frac{n_o^w}{n_o^r}$$

$$R_- = \frac{n_o^w}{n_+ + n_o^r}$$

$$n_+ + n_o^w + n_o^r = 1$$

where R_o is the wall to rod activity ratio in the absence of an electric field

R_- the ratio when the rod is 20 kv negative with respect to the wall

n_+ the fraction of Br^+

and $n_o^r + n_o^w$ the fractions of neutral bromines on the rod and wall respectively.

R_o is taken from the average of neutral ratios previously found for the geometry of the electrodes and its value is 21.[3,4] Earlier experiments have demonstrated the absence of negative Br as a product of the isomeric transition process. The n_+ values calculated from the equations are found in column 5. The 61, 76 and 60 per cent of positive atoms observed are far below the expected 100 per cent, but are within the experimental variation of the data obtained using lower voltages. The agreement of the results gives further support to the reality of the neutral bromine atoms found in this experiment. However, despite extensive study of the conditions of this experiment, some unknown factor may be responsible for their presence, for no reasonable explanation for the finding of uncharged product atoms in the internal conversion process is apparent.

TABLE VI

Exp.	C_2H_5Br Pressure (microns)	Br^{80} Activity (cts/min) Rod	Wall	Ratio (Wall/Rod)	n_t
1	4.1	1020	598	0.59	0.61
2	4.3	2655	760	0.29	0.76
3	3.7	1936	1202	0.62	0.60

2. Exchange Studies on Ethyl Acetate - Heavy Water Systems (S. Wexler)

B. Hamermesh and G. R. Ringo have recently proposed a method for determination of the capture cross section of hydrogen to an accuracy of better than one per cent. The desired accuracy may be attained with the method of the exponential pile. A hydrogen containing compound dissolved in heavy water is the diffusing medium for neutrons.

About 200 liters of very pure D_2O are used in this experiment. Because of its high cost, the water must be recovered without loss of isotopic purity. Obviously, the hydrogen compound must not exchange with D_2O and must also be readily separated from the latter. Ethyl acetate appeared to satisfy these restrictions. However, the following experiments were carried out to test the exchange of these constituents under conditions roughly simulating those to be employed in the proposed experiment. Three solutions of ethyl acetate in D_2O, two per cent ethyl acetate by volume, were prepared and allowed to stand from four to seven days. Two of the solutions were in contact with #347 stainless steel filings for the standing period and then distilled from a portion of the same filings. The filings were added in order to expose the solution to a much larger surface area than that of the still in which the 200 liters of solution are to be purified. Distillation was through a five inch Vigreux column. After the organic compound boiled over, several fractions of the heavy water distillate were taken and analyzed for isotopic purity. The D_2O content of

each cut is given in the accompanying table.

TABLE VII

Isotopic Purity of Distilled D_2O Fractions

Fraction	Per cent D_2O Exp. 1	Exp. 2*	Exp. 3*
Original	99.72	99.75	99.71
3	99.60	99.64	99.67
4	99.70	99.62	99.67
5	99.69	99.64	99.70
6	99.74		

*The ethyl acetate - heavy water solutions in these runs were in contact with stainless steel filings for seven days and then distilled from a portion of the same filings.

The heavy water content of the fractions in Experiments 1 and 3 appear to be within experimental variation identical with the original D_2O. The slight exchange indicated in the second run is thought to be due to incomplete drying of the steel filings after cleaning. Apparently, hydrogen in ethyl acetate does not exchange with heavy water under the conditions of the proposed experiment.

3. Preparation of Metallic Na^{24} from Al (n, α) Activation (S. Wexler)

In this section is described a procedure for preparation of Na^{24} as the metal after pile irradiation of aluminum nitrate. This method was originally investigated in the attempt to obtain a high enrichment of sodium activity necessary for use as a source for a molecular beam. Although the required specific activity was not achieved, it is felt that there might be interest in this relatively simple method for making metallic Na^{24}.

70 gms of $Al(NO_3)_3$ 9 H_2O were bombarded for 24 hours in the heavy water pile and then dissolved in 93 ml of conc. HNO_3, the solution being warmed to effect clearing. 185 mgs of $NaNO_3$ was then added as carrier. The solution was cooled slowly by standing for one hour and then cooled to -3° C. in a dry ice bath. Crystallized $Al(NO_3)_3$ was centrifuged off and washed with 50 ml of conc. HNO_3 previously cooled to 0° C. The combined supernatant and washings were evaporated to dryness, the very small residue taken up in 10 ml of hot water and the remaining aluminum precipitated as the hydroxide. To separate the sodium completely from the $Al(OH)_3$, two reprecipitations were necessary. The supernatants from the three hydroxide precipitations were combined and evaporated to dryness with a few drops of conc. HNO_3.

The $NaNO_3$ residue was taken up in a few drops of dilute HNO_3, transferred to the silver covered electrode (Figure 4) and evaporated to dryness. The electrode was placed so near the soft glass evacuated bulb in Figure 4 that the sodium nitrate, when held molten with a microburner, wetted the glass. The bulb contained a tungsten wire cathode which was heated by 10.5 volts A.C.[6] When the D.C. voltage was 225 volts and the $NaNO_3$ molten, the current across the glass rose to 10-12 milliamperes. After several minutes a film of metallic sodium formed near the top of the bulb. About 75 per cent of the Na^{24} activity could be separated from the aluminum by the chemical separation, while a large fraction of the sodium was electrolyzed through the soft glass barrier.

4. Hot Atom Reactions in the Pile: Organic Retentions of I_2-Benzene and C_6H_5 I-Benzene Solutions (Frances Mohr and S. Wexler)

When an iodine nucleus undergoes radiative capture, it may suffer a recoil of up to 500 ev. The energy available is far in excess of bond

6. The electrolysis apparatus is a modification of the one by R. C. Burt, J. Opt. Soc. Am. 11, 88 (1925).

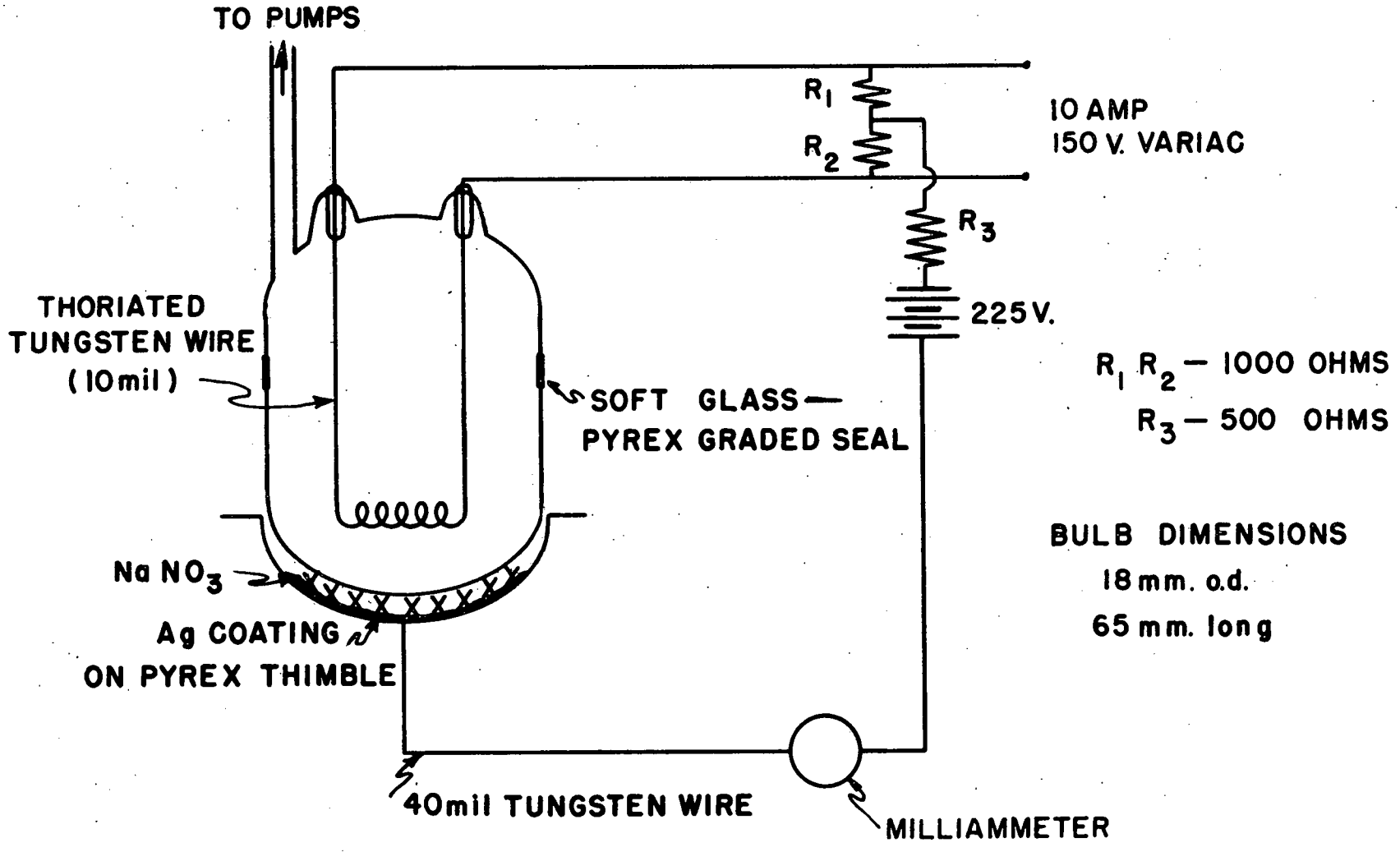

APPARATUS FOR ELECTROLYSIS OF MOLTEN $NaNO_3$

Fig. 4

energies. An organically bonded iodine atom would be freed as a result of the one or more γ-rays emitted in the process. According to recent ideas, the energetic atom in a liquid solution would escape from the liquid cage in which it was formed, be slowed down by elastic collisions with atoms of the solvent, and eventually remain unbound or react with a fragment of a solvent molecule produced by a collision.[7,8,9] Since the unattached iodine can be removed from a neutron irradiated organic liquid by extraction with suitable aqueous solutions, the fraction of iodine becoming organically united can be determined by comparison of the I^{128} activities in the organic and aqueous phases. This fraction is defined as the organic retention. We have attempted to use the experimentally determined organic retentions to study one feature of the theories of recoil reactions, namely, the escape of the radiating I^{128} atom from its bonding partner on neutron absorption. For, if the iodine concentration is sufficiently low and the recoil atom escapes from its liquid cage, the initial chemical state of the target iodine should not influence the ways in which the I^{128} combines after being slowed down to bonding energies. On the other hand, if the recoil iodine recombines with its originally linked radical, the organic retention will be greater if the iodine is initially united in an organic molecule than if it is in molecular I_2 form. Specifically, we have compared the organic retentions of irradiated I_2-benzene and phenyl iodide-benzene solutions of very low concentrations.

The procedure involved bombarding 15 ml of the solution in a small boron-free all glass tube and ground glass cover for five minutes in the "Goat Hole" of the heavy water reactor. The solution was transferred to a separatory funnel, 5 ml of carrier I_2 in benzene solution added, and the I_2 extracted into 15 ml of 0.08 M $Na_2S_2O_5$. Previously, the irradiation

7. J. M. Miller, J. W. Gryder and R. W. Dodson, J. Chem. Phys. 18, 579 (1950).
8. W. F. Libby, J. Am. Chem. Soc. 69, 2523 (1947).
9. J. M. Miller and R. W. Dodson, J. Chem. Phys. 18, 865 (1950).

vessel was rinsed out with the same bisulfite solution. The I^{128} activity of each of the two phases was measured in a high pressure ionization chamber equipped with a vibrating reed amplifier. The bombardments were monitored with a standard NH_4I solution.

The data from all runs are collected in Table VIII. Since the counting chamber was not calibrated in terms of actual disintegration rates (which is unnecessary in this experiment), the activities are in scale readings. The retentions of the initially organic bound iodine mixtures are much higher than those of the I_2 in benzene solutions. Unless there is some unknown overriding reaction, it is possible that the explanation lies in recombination of the recoiling iodine atom with its original bonding partner after the neutron activation. The results differ from those of Miller and Dodson, who found the organic retention of dilute benzene solutions of chlorine to be independent of whether the chlorine existed initially as Cl_2 or as CCl_4.[9] However, it should be pointed out that the iodine solutions studied here are about 1/100 as dilute as the chlorine employed by them.

TABLE VIII

Organic Retentions of Neutron Irradiated I_2-Benzene and C_6H_5 I-Benzene Solutions

Solution	Concentration (Mole Fraction I)	I^{128} Activity (millivolts)[a] Organic	Aqueous	Retention
I_2 in C_6H_6[b]	3.4×10^{-5}	13.5	50.2	21.2
I_2 in C_6H_6	3.4×10^{-5}	5.2	27.4	15.9
"	"	8.3	29.7	21.8
"	"	4.6	23.6	16.3
"	"	6.5	28.0	18.8
C_6H_5 I in C_6H_6	4.0×10^{-4}	29.0	81.0	26.4
"	"	35.9	85.2	29.6
"	4.0×10^{-5}	5.7	11.7	32.4
"	"	6.3	15.1	29.5
"	"	5.0	13.4	27.2

(a) Activities listed for the less concentrated solutions are for a time 25 minutes after irradiation. 75 minutes elapsed between the end of bombardment and the counting time in the 4.0×10^{-4} mole fraction C_6H_5 I solution.

(b) This solution was irradiated for one hour and then allowed to decay 75 minutes before the activity measurement.

5. Condensation of Na^{24} Molecular Beams on Various Metals (J. Dalman and S. Wexler)

In Wattenberg's design of a molecular beam apparatus for the determination of nuclear spins, the intensity of the beam is monitored by a metallic tape crosswise to the collecting wire.[10] The minute beam of radioactive nuclei is condensed on the wire and tape after leaving the magnetic field, the two collectors moved under individual end window counters, and the activity on each measured. The counting rate of the

10. J. Dalman and A. Wattenberg, ANL-4397.

collecting wire determines the intensity of the molecular beam at the original position of the wire, while the activity on the tape measures the intensity of the entire beam. Obviously, all or a constant and high fraction of the radioactive nuclei must condense on the wire and tape for this method to be useful. In this report we describe experiments made to determine the efficiency of several metal tapes for condensation of molecular beams of Na^{24}.

50 to 100 mgs of metallic sodium was irradiated to approximately half-saturation in the central thimble of the heavy water pile, the metal was transferred to a small oven and, on heating the oven, the molecular beam was located with a surface ionization detector. The beam was then allowed to fall on one of several metallic tapes for periods of thirty minutes to one hour. The amounts of Na condensed was measured through the activity of the tape after moving it to a position below an end window counter.

Tapes of nickel, brass and copper surfaces showed no activity above background when used as collectors for Na^{24} beams. However, a copper-amalgam tape yielded the activities listed in Table IX. This chemically active surface was prepared by immersing five mil Cu tape in a dilute nitric acid solution of mercury, rinsing in water and outgassing under vacuum.

TABLE IX

Na^{24} Activity on Cu-Amalgam Tape

Time of Exposure to Beam (min)	Cts/Min Above Background
30	23
60	55

Apparently, sodium atoms tend to re-evaporate from the metallic surfaces tested, with the exception of Cu-amalgam. The amalgam seems to be effective in condensing Na on first collision with the surface.

IX. Radioactive Indium Recoil Atoms (S. J. Yosim)

More experiments were run to determine whether recoil atoms emitted from indium surfaces were in the form of neutral atoms or ions. Data of the fall quarter indicated the possibility that the recoils were positively charged, since a collector which was positive with respect to the indium source contained fewer recoils than a field free collector.

During this quarter, five experiments with charged electrodes were run, the indium surface not being exposed to the atmosphere until after the irradiation. In two of these a positive 1500 volts was applied and to the other three a negative 1500 volts. The following are the data:

Chamber	+1,500 volts	-1,500 volts	Field Free
30	2,680 c/min		9,300 c/min
31	2,400 c/min		5,900 c/min
36		9,700 c/min	9,100 c/min
37		11,100 c/min	5,960 c/min
38		7,950 c/min	6,950 c/min

The above data together with the earlier data indicate the probability that the recoil atoms from an indium surface are + ions. A similar experiment will be run with gold foil as a source of recoil atoms.

X. Group #3 - M. G. Inghram

1. Krypton Content of the Atmosphere - (R. J. Hayden, M. G. Inghram)

The determination of the krypton content of the air by the mass spectrometric isotopic dilution method has given some preliminary results. There are, however, several experiments which must be completed to test for systematic errors before the results can be considered as final. The results to date indicate a value of 1.06 ± .04 ppm by pressure for dry surface air in Chicago.

The major difficulty in this type of analysis is handling small amounts of gas in a reliable and reproducible manner. The amounts of Kr used are of the order of 8×10^{-5} cc at S.T.P. There are several precautions which have been found necessary to give reproducible results with these small quantities of gas. These precautions can best be pointed out by giving a brief outline of the experimental procedure. The technique outlined can be used with appropriate modifications to analyze any gas for trace impurities.

1. Make krypton tracers by neutron irradiation of outgassed NaBr in an evacuated quartz capsule.
2. Recover tracer from NaBr by vaporization of NaBr in a greaseless, charcoal free system, and purify gas with a calcium furnace.
3. Put tracer in a greaseless, charcoal free systeme containing a number of sample tubes (break-off type) whose volume ratio is known and which can be isolated from one another simultaneously by mercury cutoffs.
4. After complete mixing and equilibrium has been established, isolate the individual tubes with the cutoff and seal off the tubes with a torch.

5. Prepare standard spectroscopically pure (Linde) krypton sample of known volume and pressure by use of a modified McLeod.
6. Mix one of the tracer tubes with the standard krypton and measure the mixture on the mass spectrometer to get the ratio of the amount of tracer krypton to Linde krypton. Thus knowing the amount of tracer in one sample and knowing the ratio of its volume to the other tracer samples one knows the amount of Kr tracer in each tracer sample tube.
7. Repeat step 6 with several other samples to check for statistical errors.
8. Take an outdoor air sample of $\sim$ 80 cc by breaking off an evacuated vessel. Reisolate with a mercury cutoff and seal off with a torch.
9. Mix this known volume of air with one of the now known krypton tracers still in a greaseless charcoal free system. After mixing is completed, remove the gross gas O_2 and N_2 by treating with Ca. Measure the resulting krypton in the mass spectrometer to get the ratio of the amount of tracer to the amount of air krypton and hence the krypton content of the atmosphere.
10. Repeat step 9 with other samples to check for statistics.

The major source of systematic error is gas absorption even in these "clean" systems. We are at present trying to evaluate these errors by using tracer samples having quite different surface to volume ratios.

2. Pu^{240} Half-Life - (D. C. Hess, M. G. Inghram)

In cooperation with the Chemistry Division, the samples of plutonium and uranium milked from plutonium samples (see ANL-4469,p.7) have been rerun

on the new high resolution 12" single focussing mass spectrometer. The results were in essential agreement with the results of the older machines (using 24,410 years for the 239 half-life). The final value for the half-life of Pu^{240} is 6600 plus or minus about 1 percent.

3. Pu Analyses - (D. C. Hess, M. G. Inghram)

A sample of Chalk River Pu was analyzed in order to compare the cross section of Pu^{240} in a slug with that observed by bombarding separated Pu^{239} in a slow flux. The computed ratio of the 239 to 240 cross sections are somewhat higher than those observed for slow fluxes. The isotopic composition of the Chalk River material is

$$Pu^{239} = 93.71 \pm .06$$
$$Pu^{240} = 5.77 \pm .06$$
$$Pu^{241} = 0.453 \pm .004$$
$$Pu^{242} = 0.020 \pm .004$$

4. Lead Uranium Analyses - (C. Patterson, G. Tilton, H. Brown, D. C. Hess & M. G. Inghram)

A new method of lead isotopic analysis has been developed which required only 5 micrograms of lead for an analysis as compared to previous 1000 microgram minima. The method has been used for uranium lead age determination in rocks containing down to 1 ppm of uranium. Perhaps the most interesting point which has been uncovered in this work is that igneous rock which contains 4 ppm of uranium has about half of that uranium in the mineral zircon which is present to only 0.1%. This suggests that in low grade ores, rather than extracting uranium as such, a much simpler procedure would be to first extract zircon by flotation. This would improve the ore by a factor of about a thousand, and considerably simplify

the later purification. Two samples of lead extracted from petrified bones in the Colorado carnotite region were also analyzed by this method at the request of the AEC, in an attempt to get some clue to the mechanism of the Colorado uranium deposits.

5. Double Direction Focussing Mass Spectrometer - (D. C. Hess, M. G. Inghram)

The adjustment of the new double direction focussing mass spectrometer is continuing. In the process, five new isotopic limits were obtained - $La^{137} < .0002\%$; $Sm^{142} < .0001\%$; $Sm^{143} < .0001\%$; $Sm^{145} < .0001\%$; $Sm^{146} < .0002\%$. These are 10, 10, 20, 20 and 10 times respectively more sensitive than any previous instrument. The limits recorded here were limited by ion intensity, not resolution as is the usual case. Thus addition of an electron multiplier of which we have models operating with gains of 10^5 should give us the sensitivity of the order of 10^{-8} which is the design figure.

XI. Group #4 - W. H. Zachariasen

1. Crystal Chemistry of Protactinium

A. Protactinium Metal - (W. H. Zachariasen, H. A. Plettinger)

The crystal structure of protactinium metal has been determined. The tetragonal body-centered unit cell containing two atoms has dimensions

$$a_1 = 3.925 \pm 0.005 \text{ Å}, \qquad a_3 = 3.238 \pm 0.007 \text{ Å}.$$

The calculated density is $\rho = 15.37 \pm 0.08$.

The coordination number is ten. The results show that there are no 5f electrons in protactinium metal.

Details are given in a special report.

B. PaH_3

A phase isostructural with UH_3 was found in a sample of protactinium metal treated with hydrogen. This phase must accordingly be PaH_3. The unit cell constant is $a = 6.648 \pm 0.010$ Å.

2. Study of Zirconium Fluorides - (W. H. Zachariasen, H. A. Plettinger)

By treating zirconium hydroxide with HF I have prepared three different hydrates of zirconium fluoride. These are $ZrF_4 \cdot 4H_2O$, $ZrF_4 \cdot 3H_2O$ and $ZrF_4 \cdot H_2O$. Samples of these phases have been submitted for chemical analysis, but no results have as yet been received. The given formulas are based upon the determination of the zirconium percentage which I have carried out myself.

Preliminary results of x-ray studies of these compounds are:

A. $ZrF_4 \cdot 3H_2O$

Orthorhombic base-centered unit cell with

$$a_1 = 6.64\ \text{Å}, \qquad a_2 = 9.88\ \text{Å}, \qquad a_3 = 8.08\ \text{Å}$$

and four molecules per unit cell.

B. $ZrF_4 \cdot H_2O$

Tetragonal body-centered with

$$a_1 = 7.70\ \text{Å}, \qquad a_3 = 11.68\ \text{Å}$$

and eight molecules per unit cell.

I have studied the hydrolysis of $ZrF_4 \cdot H_2O$. Two oxyfluorides exist, namely Zr_2OF_6 and $ZrOF_2$. The chemical formula of the former is deduced from chemical analysis of zirconium and fluorine carried out by the analytical section of the Chemistry Division. The formula $ZrOF_2$ is based upon a zirconium determination of my own.

Preliminary crystallographic results are:

C. Zr_2OF_6

Orthorhombic face-centered with $a_1 = 9.64$ Å, $a_2 = 6.63$ Å, $a_3 = 7.94$ Å and four molecules per unit cell.

D. $ZrOF_2$

The structure of $ZrOF_2$ is related to that of hexagonal UO_3. However, $ZrOF_2$ is orthorhombic. A pseudo-cell containing two molecules has these dimensions:

$$a_1 = 6.45\ \text{Å}, \qquad a_2 = 3.84\ \text{Å}, \qquad a_3 = 4.08\ \text{Å}.$$

979-43-

A-2442

3. Thorium Fluorides - (W. H. Zachariasen, H. A. Plettinger)

I reported in an earlier report that $ThF_4 \cdot \frac{1}{3}H_2O$ was prepared. Further study showed that the phase in question is the anhydrous tetrafluoride. It does not seem to have been known that ThF_4 can be prepared in anhydrous form in the wet way. The conditions under which anhydrous ThF_4 were obtained are briefly as follows:

A hot concentrated solution of thorium nitrate was precipitated with 48% hot HF-solution. To obtain the anhydrous form the temperature of the solutions should be about 90°C. The precipitate was washed and dried at 95°C.

It should be remarked that UF_4 cannot be obtained in anhydrous form according to this method. Experiments with boiling solutions have invariably given $UF_4 \cdot H_2O$.

Wahl et al

979-44

~~A-2144-3~~

XII. Discrepancies in Nuclear Shell Theory (H. H. Hummel)

Two discrepancies in the shell theory of light nuclei are being examined in collaboration with D. R. Inglis. In F^{19} an $s_{\frac{1}{2}}$ level occurs as the ground state, instead of $d_{5/2}$ as expected, and in N^{13} the first excited state is believed to have even parity instead of odd as expected.

In order to check this latter point, data on the scattering of protons from C^{12}, obtained at Wisconsin by G. Goldhaber and R. Williamson, to be published in the Physical Review, were examined. The shape of the resonance corresponding to the first excited state of N^{13} appears to require an s proton incident, in violation of what would be expected from the theory. This merely confirms what is generally believed.

Some attempts have been made without success to alter in the required way the order of the levels of a single particle in a central field by varying the radial dependence of the potential. Apparently what is required is a function rising steeply at the origin. The question of whether the desired result can be achieved in a physically reasonable way has not yet been answered.

Inelastic Scattering From Li^7

The failure of the second excited state of Li^7 to show up in the inelastic scattering of Li bombarded by deuterons and α-particles (Gove and Harvey, to be published in Physical Review) is being studied in collaboration with D. R. Inglis. If one calculates transition probabilities based on only an electrostatic interaction between the bombarding particle and the last proton in Li^7, it is found that the second excited state is only one-sixth as likely to appear as the first. However, the probability that the first state will be excited is one hundred times too small.

XIII. Calculation of the Field of the Lens System of the Linear Accelerator (E. Hellund)

The Argonne accelerator has a tube of 65 successive electrostatic lenses preceded by a focussing section which starts the ions toward the target with a kinetic energy of about 55 to 85 kev. The focussing section is just a cylinder 10 inches long with a diameter of 1 3/4 inches. This cylinder actually consists of two separate insulated cylinders of 3 inches and 7 inches. The short section and connectors furnish a so-called "field free" region to the first of the series of electrostatic lenses. The following diagram is schematic only:

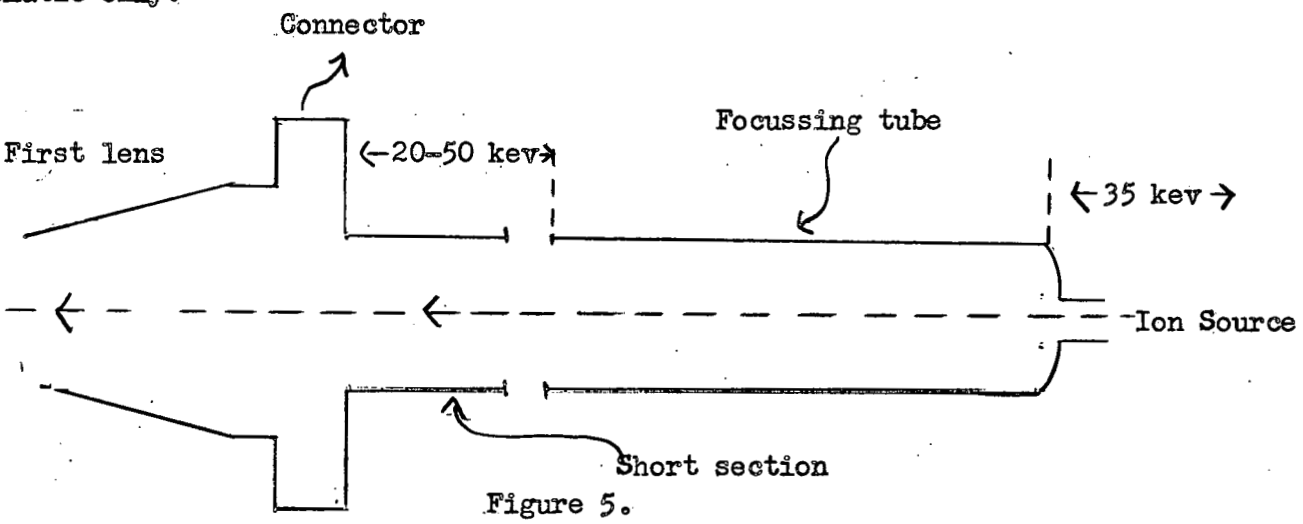

Figure 5.

The entire length of the first lens plus connectors plus the short section of the focussing tube is all at the same potential.

The first lens action is that taking place at the junction of the two sections of the focussing tube. From the point of view of a boundary value problem, it furnishes the starting slope and radial displacement for motion down the tube.

Basically the entire lens system is composed of elements of the same type. That is, we need investigate only the design consisting of coaxial cylinders of equal diameter.

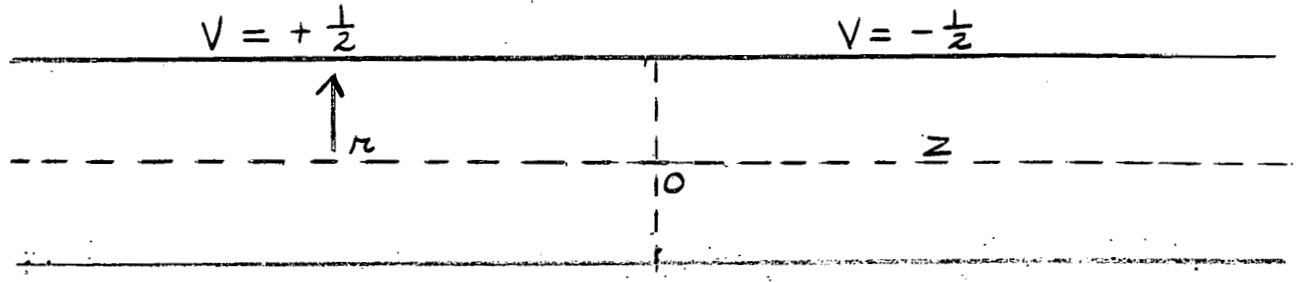

Figure 6.

Actually the lenses which make up the main accelerating tube are truncated cones, but the generators are practically parallel to the axis of the tube and are, furthermore, quite distant from the axis. One may expect, therefore, that for the particles whose trajectories run close to the axis the focussing predictions based on the use of the lens of Figure 6 will be quite accurate. On the other hand, for those particles that move far out from the axis, increasing errors will infiltrate the calculations. It is just the latter particles that contribute to spherical aberration. For these, the equations of motion are non-linear and hence the roots (points of intersection with the axis) are functions of the initial slope as well as the initial point of emission.

Returning now to Figure 6 we evaluate the potential distribution for a drop of 1 volt from one lens to the next,

$$V(r,z) = -\frac{1}{\pi}\int_0^\infty \frac{\sin(kz)}{(k)} \quad \frac{J_0(ikr)}{J_0(ikR)}\, dk \qquad (1)$$

where R is the radius of the cylinders, and J_0 designates the Bessel function of order zero.

In the event that the cylinders are separated by a distance of "2a", the solution is

(2)

$$V(r,z) = -\frac{1}{\pi a}\int_0^\infty \frac{\sin(ak)\sin(kz)}{k^2}\,\frac{J_0(ikr)}{J_0(ikR)}\,dk$$

The unfortunate circumstance in regard to the above two formulae is that the expressions require numerical integration. It is, therefore, of practical interest to devise a simpler approximate procedure which will yield reasonably accurate solutions in a form facilitating rapid computation. Some numerical work is available on the evaluation of (1) and (2) which may be used as a check on our approximate procedure.

Mathematical Analysis

The Laplacian for axially symmetric fields is

$$\frac{\partial^2\phi}{\partial z^2} + \frac{1}{r}\,\frac{\partial}{\partial r}\left(r\,\frac{\partial\phi}{\partial r}\right) = 0 \qquad (3)$$

where r and Z have the usual meanings and ϕ represents the potential.

Solving (3) for the radial field strength E_r in terms of the Z component of the field, E_Z, we obtain

$$E_r = -\frac{1}{r}\,\frac{\partial}{\partial z}\int_0^r (rE_z)\,dr \qquad (4)$$

One may infer directly from (4) under the assumption of small "r" and slow variation of $\frac{\partial E_z}{\partial z}$, that

$$\frac{\partial E_r}{\partial r} + \frac{1}{2}\,\frac{\partial E_z}{\partial z} \simeq 0 \qquad (5)$$

or, in terms of ϕ

$$\frac{\partial^2\phi}{\partial r^2} + \frac{1}{2}\,\frac{\partial^2\phi}{\partial z^2} \simeq 0 \qquad (6)$$

Adopting a new variable,

$$2^{\frac{1}{2}} z \equiv z \tag{7}$$

we obtain finally,

$$\frac{\partial^2 \phi}{\partial r^2} + \frac{\partial^2 \phi}{\partial z^2} \simeq 0 \tag{8}$$

Hence, in solving problems of axial symmetry, we may use the theory of conformal representation provided the results are used subject to the restrictions used in deriving (8).

We shall now return to the lens of Figure 6, solving (8) by means of the Schwarz-Christoffel theorem and comparing the results with available numerical work on (1).

For convenience we shall raise the potential by 1/2 volt so that the diagram in the $\bar{z}$ plane, ($\bar{z} \equiv r + i\,z$), appears,

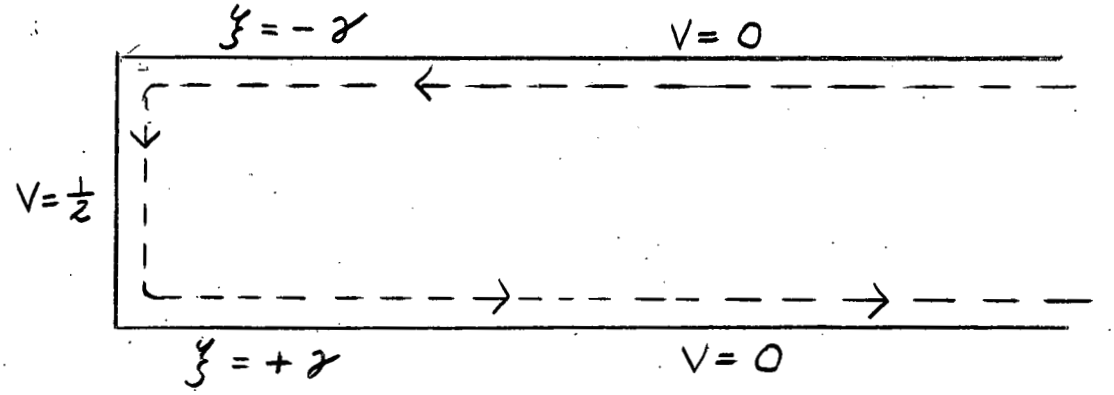

Figure 7.

and map this semi-infinite rectangle on the real axis of the intermediate ζ plane by means of the following transformation,

$$\int \frac{d\zeta}{\sqrt{\zeta^2 - \gamma^2}} = A(\bar{z} + \bar{z}_0) \tag{9}$$

integrating,

$$\log\left[\zeta + \sqrt{\zeta^2 - \gamma^2}\right] = A(\bar{z} + \bar{z}_0) \tag{10}$$

Evaluation at $\zeta = \pm \gamma$ defines A,

$$A = \frac{\pi}{2R} \tag{11}$$

where R, as before, denotes the radius of the cylinder.

Now the ζ plane is to be mapped on the W plane so that the segment of the real axis of the ζ plane from $-\gamma$ to $+\gamma$ shall correspond to the line U+i $(\frac{1}{2})$ in the W plane.

The proper mapping function is

$$W = \frac{1}{2\pi} \log \left[\frac{\zeta - \gamma}{\zeta + \gamma} \right] \tag{12}$$

Further, selecting $\bar{Z}_o$ so that the left boundary of the semi-infinite rectangle corresponds to $z = 0$, and lowering the whole potential by $\frac{1}{2}$ volt to correspond to Figure 6, one arrives at,

$$W = \frac{1}{\pi} \log \left[\tan \left\{ \frac{\pi}{4} - i \frac{\pi}{4R} (2^{\frac{1}{2}} Z + i r) \right\} \right] \tag{13}$$

Along the axis, $(r = 0)$,

$$V = -\frac{2}{\pi} \tan^{-1} \left\{ \tanh \left(\frac{\pi Z}{2^{3/2} R} \right) \right\} \tag{14}$$

$$\frac{\partial V}{\partial (Z/R)} = \frac{-\left(2^{\frac{1}{2}}\right)}{\cosh^2 \left(\frac{\pi Z}{2^{3/2} R} \right) + \sinh^2 \left(\frac{\pi Z}{2^{3/2} R} \right)} \tag{15}$$

Formulae (14) and (15) are now compared with actual numerical evaluation of (1). The results appear in Figure 8.

The agreement is seen to be quite satisfactory. Formulae (14) and (15) yield accurate plots of the refractive index along the axis, and (13) may be expected correspondingly to yield acceptable results for small "r" values.

Now to obtain the transformation for a series of lenses, (ignoring end

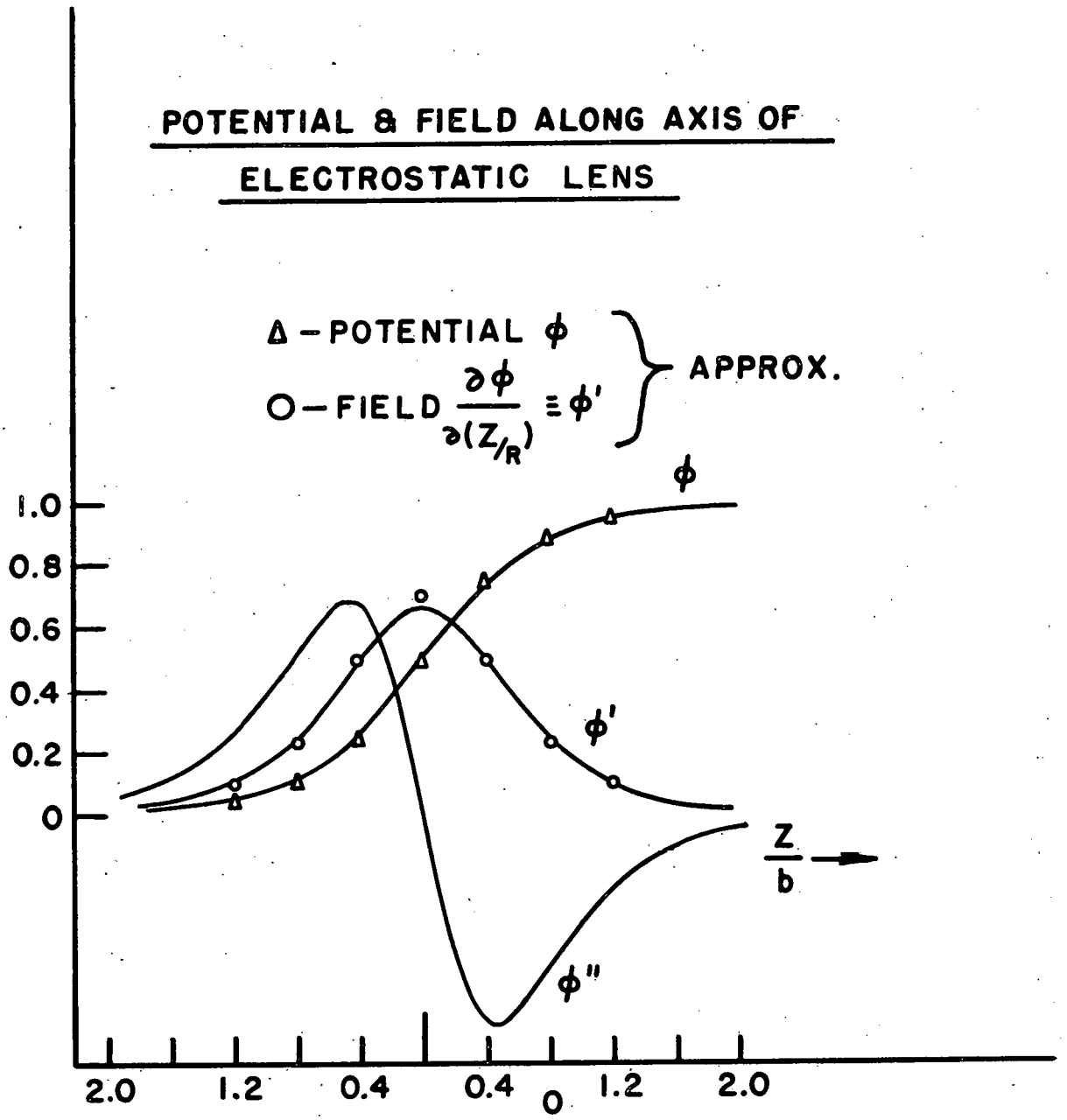
POTENTIAL & FIELD ALONG AXIS OF
ELECTROSTATIC LENS
Δ – POTENTIAL φ
O – FIELD ∂φ/∂(Z/R) ≡ φ'
APPROX.
φ
φ'
φ''
1.0
0.8
0.6
0.4
0.2
0
Z/b
2.0
1.2
0.4
0.4
0
1.2
2.0

Fig.8

979-5k

effects), one may simply add the W given by (11) for each lens gap

$$W = \frac{V_o}{\pi} \sum_j \left[\log \tan \left\{ \frac{\pi}{4} + \frac{\pi}{4}\left(\frac{r}{R}\right) - \frac{i\pi}{2^{3/2}} \frac{(z - jd)}{R} \right\} \right] \tag{16}$$

where j takes on positive and negative integer values, and "d" is the length of each lens.

V_o is now the voltage drop from lens to lens.

In actual practice, the series (16) converges so rapidly, that only two lenses on each side of the one considered need be retained to compute the radial field responsible for focussing.

Concluding this discussion, one may state the final problem, which is, to compute the trajectory in the focussing tube and acceleration tube, subject to the fields given by (13) and (16). The calculation is to be made on the basis of a linearized equation of motion since only very narrow pencils of rays will permit the definition of an image free of aperture defect, (spherical aberration).

XIV. Axial Asymmetry in the Linear Accelerator (E. Hellund)

Introduction

As is well known, production of refractive heterogeneity is a consequence of the penetration of any stray field into the lens system of a linear accelerator. Any such effect could lead to troublesome perturbations in focussing properties of the tube.

In the case of the electrostatic generator, an elementary calculation shows that the belt charge is at times so large as to make possible a deflection in the proton beam of the order of two meters for an unshielded path.

It is, of course, true that the accelerated particles are partially shielded by the successive electrostatic cylindrical lenses, but the interval spacing is so large that one might suspect the shielding to be inadequate to prevent deflections of the order of a centimeter. To produce such a displacement would require penetration of only 1/2000 of the field due to the belt charge.

The gap between successive lenses is about $2\frac{1}{2}$ inches, beginning at a distance of 5 inches from the axis. Actually, the beam is "shaded" from any field coming directly through this channel by the cylindrical bands forming the real lenses. Still, the mean open channel width through the space between lenses is about $1\frac{1}{2}$ inches in an overall length of about $4\frac{1}{2}$ inches.

In the following, the problem of penetration in such channels has been treated for the two dimensional field. Change from three to two dimensions considerably simplifies the analysis although at the expense of depriving one of a simple correspondence between the transmissions in the two cases.

Mathematical Analysis

One considers the array in the Z-plane,

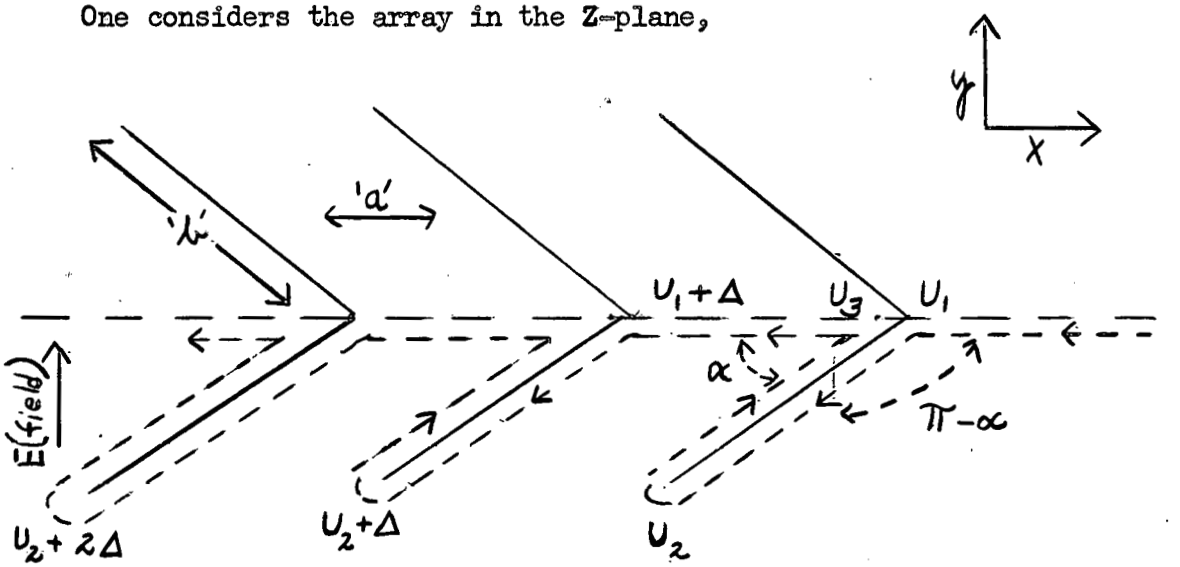

Figure 9.

Where the correspondence with the points in the W-plane is indicated as for an infinite series of wedge shape lenses of zero aperture. The actual lenses are of the following appearance:

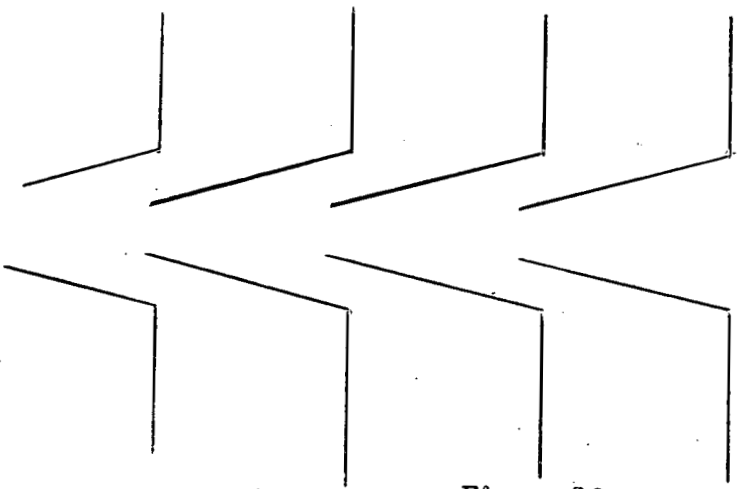

Figure 10.

However, as will be shown in calculations on the geometry of Figure 9, the penetration is a function solely of the ratio of length to width of the channel, and is independent of the orientation of the external field. We shall therefore multiply the transmissions for succeeding channels although this is not rigorously accurate since the successive incident fields are perturbed.

Returning to Figure 9, it may be seen that symmetry allows one to map just half of the plane.

Employing the Schwarz-Christoffel theorem, with the Weierstrass factor theorem, one may show without difficulty that the correct mapping function is,

$$-E = \left(\frac{dW}{dz}\right)\left[\sin\left\{\frac{\pi}{\Delta}(w-U_1)\right\}\right]^{-\alpha/\pi}\sin\left\{\frac{\pi}{\Delta}(w-U_2)\right\}\left[\sin\left\{\frac{\pi}{\Delta}(w-U_3)\right\}\right]^{-1+\alpha/\pi} \tag{1}$$

where E is the strength of the electric field.

For $|y| \to \infty$, $|v| \to \infty$, one obtains,

$$-E \simeq -E\, e^{-\frac{\pi}{\Delta}\left[\frac{\alpha}{\pi}U_1 - U_2 + (1-\frac{\alpha}{\pi})U_3\right]} \tag{2}$$

which leads to the following restriction on U_1, U_2, U_3,

$$\frac{\alpha}{\pi}U_1 - U_2 + \left(1-\frac{\alpha}{\pi}\right)U_3 = 0 \tag{3}$$

If one now adopts new variables,

$$\begin{aligned}\theta &= \frac{\pi}{\Delta}(w-U_1)\\ \theta_3 &= \frac{\pi}{\Delta}(U_3-U_1)\\ \theta_2 &= \frac{\pi}{\Delta}(U_2-U_1)\\ \theta_1 &= \frac{\pi}{\Delta}(U_1-U_1)\equiv 0\end{aligned} \tag{4}$$

we obtain,

$$-E\,\frac{\pi}{\Delta} = \frac{d\theta}{dz}(\sin\theta)^{-\frac{\alpha}{\pi}}\sin(\theta-\theta_2)\left[\sin(\theta-\theta_3)\right] \tag{5}$$

with

$$\left(1-\frac{\alpha}{\pi}\right)\theta_3 = \theta_2 \tag{6}$$

For simple disc shaped lenses, $\alpha = \frac{\pi}{2}$ we have

$$\theta_3 \Big]_{\alpha = \frac{\pi}{2}} = 2\,\theta_2 \tag{7}$$

The latter statement merely confirms the physically obvious conclusion that, in such a case, as many field lines terminate upon one side of the lens as upon the other.

With the choice of variables of (4) one may easily recognize that the percentage of the transmitted field is,

$$\begin{matrix}\text{fraction} \\ \text{trans. field}\end{matrix} \equiv \frac{\pi - \theta_3}{\pi} \tag{8}$$

Where θ_3, and θ_2 are fixed by (6) and the geometry of the lens system (i.e., by the ratio of b/a).

Insertion of the lens specifications is facilitated by the fact that the transmitted field is small,

$$\pi - \theta_3 \equiv \epsilon \longrightarrow 0 \tag{9}$$

Writing,

$$\beta \equiv \alpha + \epsilon\left(1 - \frac{\alpha}{\pi}\right); \quad \pi - \beta = \theta_2 \tag{10}$$

and

$$I = \int_0^{\pi-\beta} (\sin x)^{-\frac{\alpha}{\pi}} \sin(x+\beta)\left[\sin(x+\epsilon)\right]^{-1+\frac{\alpha}{\pi}} \tag{11}$$

one may show by elementary means that,

$$\frac{\partial I}{\partial \epsilon} = -\frac{\left[\sin\left\{\alpha + \epsilon\left(1 - \frac{\alpha}{\pi}\right)\right\}\right]^{1-\gamma}\left[\sin\left\{\alpha - \epsilon\,\frac{\alpha}{\pi}\right\}\right]^{\gamma}}{\sin(\epsilon)} \tag{12}$$

Where the above relation is exact and does <u>not</u> demand that ϵ be small. However, in the limit of $\epsilon \to 0$

$$I(\epsilon) = -(\sin\alpha)\log\epsilon + \text{const} + o(\epsilon) \tag{13}$$

As may be seen by consulting (5), $I(\epsilon)$ furnishes the scale of "b". Integrating (5) from θ_3 to π then inserts the lens spacing.

$$\int_{\pi-\epsilon}^{\pi} (\sin x)^{-\frac{\alpha}{\pi}} \sin(x+\beta)\sin(x+\epsilon)^{-1+\frac{\alpha}{\pi}} dx \simeq \pi + O(\epsilon^2) \tag{14}$$

Finally, therefore,

$$\begin{matrix}\text{fraction}\\ \text{of transmitted}\\ \text{field}\end{matrix} \simeq e^{-\left(\frac{\pi b}{(\sin\alpha)a}\right)} \tag{15}$$

It may be noticed that (15) can be written in simpler fashion as

$$e^{-(\pi)\left(\frac{L}{W}\right)} \tag{16}$$

where $L \equiv b$ is the length of the channel and W is the width (perpendicular). Finally, the product of the transmissions of the two sections making up the entire channel, (Figure 10), on inserting numerical values, yield,

$$\sim e^{-\pi\left[1+\frac{2}{(\frac{1}{2})}\right]} \simeq e^{-15} \sim 10^{-6}$$

The transmitted field, therefore, can not be regarded as physically significant.

XV. Electron Recombination and the Mobility of Helium Ions in Helium

(R. E. Meyerott)

It has recently been pointed out by Bates[1] that the electron recombination coefficient and the ambipolar diffusion coefficient reported by Biondi and Brown[2] are apparently contradictory. The electron recombination coefficient reported must be that of He_2^+ since it is about 10^4 times larger than one would expect for He^+, while the ambipolar diffusion coefficient reported gives a value of the mobility of helium ions in helium of 13.7 cm^2/volt sec. in agreement with the value 13 cm^2/volt sec. reported by Tyndall and Powell[3] in 1930. It has been previously suggested[4] that this value is probably the mobility of He^+ in helium, while the value 21.4 cm^2/volt sec. reported by Tyndall and Powell[5] in 1931 is the mobility of He_2^+ in helium. Biondi and Brown[2] have also suggested that their value refers to the mobility of He^+ in helium. Thus it would appear that the measurement by Biondi and Brown of the electron recombination coefficient was that of He_2^+, while at slightly lower pressures the measurements of the ambipolar diffusion coefficient was that of He^+.

These results are not necessarily contradictory, for the electron recombination coefficient was measured at gas pressures of 28.7 mm and 21.2 mm and initial electron concentration about $10^{11}/cm^3$, while the ambipolar diffusion coefficient was measured at pressures from 2 mm to 12 mm and electron concentration of about $10^9/cm^3$. Not much is known about how the helium molecular states are formed in discharges at high pressures, but it seems likely that the metastable molecule He_2^* is formed first and then later ionized to form He_2^+. The molecule formation involves a two or three-body

1. D. R. Bates, Phys. Rev. 77, 718 (1950)
2. M. A. Biondi and S. C. Brown, Phys. Rev. 75, 1700 (1949); Phys. Rev. 76, 302 (1949)
3. A. M. Tyndall and C. F. Powell, Proc. Roy. Soc. A129, 162 (1930)
4. R. Meyerott, Phys. Rev. 66, 242 (1944)
5. R. Meyerott, Phys. Rev. 70, 671 (1946)

collision, so that the probability of formation is proportional to the square or cube of the pressure. If the molecule ion formation is a two-stage process, the number of molecule ions will vary as the square of the electron concentration used to excite the gas. There is some indication[5] in discharge tubes somewhat larger than those used by Biondi and Brown that the number of metastable molecules approximately equals the number of metastable atoms at pressures of about 3 mm. Hence, we might expect that the number of He_2^+ ions exceeded the number of He^+ ions in the Biondi and Brown measurement of the electron recombination coefficient, while the reverse was true under the conditions at which the ambipolar diffusion coefficient was measured.

In addition, these experiments are highly selective. Since the electron recombination coefficient of He_2^+ is apparently $\sim 10^4$ times that of He^+, even in a mixture of 50% He^+ and 50% He_2^+ essentially what is observed is that of He_2^+! The ambipolar diffusion coefficient is measured by observing what amounts to the decrease of the number of positive ions with time. The ions with the highest mobility disappear first. If one waits long enough after the discharge has been turned off to observe the ambipolar diffusion, most of the ions of high mobility, He_2^+, will have diffused to the walls, and only those of low mobility, He^+, will be left.

XVI. Potential Fields Around Ions in High Temperature Gas Mixtures

(G. Keller* and R. E. Meyerott)

Preliminary to the calculations of the radiative opacity of gas mixtures of astrophysical interest, a study has been made of the potential fields in the neighborhoods of gaseous ions, with particular emphasis on the effects due to adjacent ions.

Methods used heretofore have assumed that each ion is enclosed in a spherical volume of radius a_z (Ref. 1), wherein no other ions are permitted. This is of course, only a first approximation. Using a generalized Thomas-Fermi method it has been found that, for pure iron at 11.6 million degrees and with three bound electrons, the density of neighboring ions at a distance of $1/2a_z$ from any particular ion is still appreciable. For a gas mixture of the proportions suggested by Harrison Brown[2] the densities of H, He, O and Fe ions at $1/2a_z$ are 76, 57, 13 and 0 percent of the respective average densities. The accompanying depression of the ionization potentials is only 60 percent of that computed by Morse's method.

---

1. Marshak, Morse and York, Ap. J. 111, 214, (1950)

2. H. Brown, Rev. of Mod. Phys. 21, 625, (1949), Table III

* Perkins Observatory

XVII. Photon Absorption Coefficients of Light Elements and Mixtures (R. E. Meyerott and S. A. Moszkowski)

Abstract - The problem considered was to find a mixture of elements which acts as a filter for radiation by absorbing thermal radiation corresponding to a temperature of 1 to 2 kev, but transmits radiation of higher frequency.

For cases of high temperature and low density, the equations for the various absorption and scattering coefficients take a simple form. These equations are discussed and it is estimated what mixtures have the desired property of being a filter.

The complete report of this abstract will be published as ANL-4594.

XVIII. Interim Progress Report on the ORNL Digital Computer (J. C. Chu)

The interim report on the status of the digital computer is to appear as ANL-4600. The report contains a discussion of the logical design of the machine and of research and development work to date.